2014

Top-loading Small-sample Calorimeters for Measurements as a Function of Magnetic Field Angle

Nathanael Alexander Fortune
Smith College, nfortune@smith.edu

Scott T. Hannahs
National High Magnetic Field Laboratory

Top-loading small-sample calorimeters for measurements as a function of magnetic field angle

Journal of Physics: Conference Series **568** (2014) 032008 doi:10.1088/1742-6596/568/3/032008

Top-loading small-sample calorimeters for measurements as a function of magnetic field angle

N A Fortune[1], S T Hannahs[2]

[1] Department of Physics, Smith College, College Lane, Northampton MA 01063, USA
[2] National High Magnetic Field Laboratory, Florida State University, 1800 E. Paul Dirac Road, Tallahassee FL 32310, USA

E-mail: nfortune@smith.edu

Abstract. In quasi-low-dimensional systems, the existence of a particular physical state and the temperature and magnetic-field-dependence of its phase boundary often strongly depends on magnetic field orientation. To investigate magnetic field orientation dependent phase transitions in these materials, we have developed rotatable miniature and sub-miniature sample-in-vacuum calorimeters that operate in dc magnetic fields up to 18 and 45 tesla. The calorimeters cover the temperature range from below 0.1 K to above 10 K; they are able rotate a full 360 degrees relative to the applied magnetic field while remaining at base temperature. Samples are typically on the order of 1 mg in mass and up to 2 mm^2 x 0.5 mm in volume.

1. Introduction

The ability to rotate a sample relative to an applied magnet field offers a number of advantages for high field, low temperature specific heat and magnetocaloric measurements, including (1) more accurate alignment of the field along one or more crystal axes [1, 2, 3], (2) the opportunity to investigate strongly field-orientation-dependent novel superconducting and magnetic phases [4, 5], and (3) a method of establishing the gap structure of anisotropic superconducting ground states [6, 7, 8]. Field-orientation-dependent calorimetric measurements are especially useful for the study of layered structure and/or quasi-low dimensional materials. Recent examples include layered-structure heavy-fermion superconductors [2, 9, 10, 11, 12] and quasi-2D molecular superconductors [13, 14, 15]. In our experiments, we use a pair of calorimeters designed to fit inside the National High Magnetic Field Laboratory (NHMFL) top-loading dilution refrigerator single-axis rotating sample probes [16]. The dilution refrigerators have a cooling power of approximately 400μW at 0.1 K and a maximum cooling power of 4 mW; the very-low friction rotating stages at the bottom of the probes allow for a full 360 degrees of rotation (with a resolution of 0.020°) at base temperature. The SCM1 dil fridge incorporates an 18 T superconducting magnet; the PDF portable dilution refrigerator fits inside the NHMFL's 32 mm bore 36 T resistive and 45T hybrid magnets. The calorimeters can be used for field-dependent magnetocaloric [17], ac calorimetric [18] and thermal-relaxation calorimetric [19] measurements at temperatures between 0.1 K and 10 K. Samples are typically on the order of 1 mg in mass and up to 2 mm^2 x 0.5 mm in volume.

2. Calorimeter Design and Performance

2.1. Vacuum constraints

Our measurements require the sample to be in vacuum even though the housing is immersed in liquid helium (and is exposed to He vapor during the entire loading process). We accomplish this by compressing an indium gasket between matching step edges in the calorimeter base and cap [2] at room temperature, resulting in a superfluid-He leak-tight seal. A photo of the interior of a PDF calorimeter cap (with indium gasket resting on the interior step edge) is shown in figure 1, a top view of the calorimeter assembly, platform, base and step edge is shown in figure 2, and a close up view of the calorimeter platform and sample assembly is shown in figure 3. A locknut threads into the cap behind the base, drawing the pieces together as it advances.

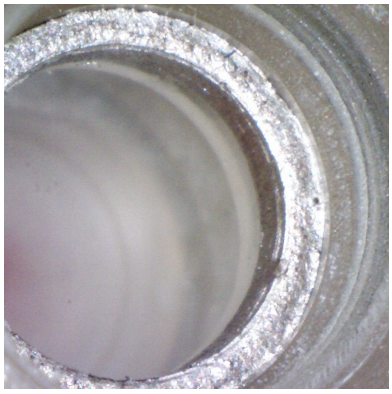

Figure 1. PDF calorimeter cap interior, showing sample chamber, step edge, indium gasket, and internal threads.

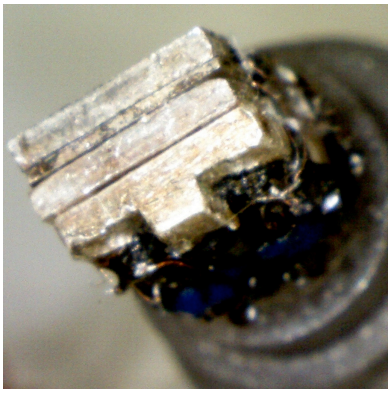

Figure 2. Top view of temperature regulated platform, and Ag sample thermometer/ spacer, and heater frames.

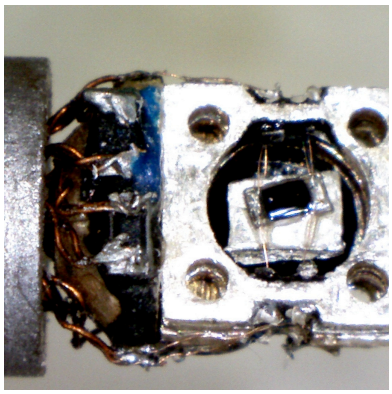

Figure 3. side view of PDF calorimeter platform and the heater/sample/thermometer sample assembly (& frames).

A vacuum is formed below 30 K by cryopumping of the air inside the housing [1]. The absence of a leak at low temperature is readily checked by measuring the heater power required to raise the interior temperature controlled platform well above that of the external cryogenic bath.

2.2. Space constraints

The calorimeter needs to (1) fit within the rotator body and (2) freely rotate 360° inside the mixing chamber of the dilution refrigerator. To accomplish this, we require that no part of the calorimeter (including leads) extend beyond the outer radius of the tip of the top loading probe at any point during the rotation. For a cylindrical calorimeter of diameter ϕ and length L rotating about a horizontal axis within a vertically aligned cylinder of diameter d, this requires that $L < \sqrt{d^2 - \phi^2}$. For the PDF rotator probe (with $\phi = 7.5$mm), $L \leq 12$mm (including room for leads). The alignment of the calorimeter within the rotator body can checked by sliding a tight-fitting clear plastic tube over the probe end and rotating the calorimeter 360°.

Once the external diameter is known, the largest possible inner diameter for the calorimeter cap is set by the minimum wall thicknesses of the indium gasket without fracturing of the housing or threads. For our PDF calorimeter constructed out of Stycast 1266 epoxy, the inner diameter of the cap is 4.2 mm (0.165 in). In practice, this limits the effective diameter of the PDF calorimeter sample assembly, supporting frames, and calorimeter platform (including sensors and wiring) to 3.5 mm (0.140 in), half what is available in the SCM calorimeter [2]. In that earlier design, the sample assembly is attached to a single 2.5 mm inner diameter (3.5 mm outer diameter) circular saphhire frame, surrounded by electrical leads heat sunk to the 7 mm diameter Ag platform. The reduced interior space available in the PDF calorimeter prompted us to try

adifferent design: in this new calorimeter, we mount each component of the sample assembly sample heater, sample, and sample thermometer on a separate frame with integrated electrical contacts, then flip the orientation of the sample assembly by 90° relative to the calorimeter's longitudinal axis, as shown in figure 3. This gives us a 2 mm diameter sample space (compared to 2.5 mm before); the 3 frame design can accommodate samples up to 0.5 mm in thickness.

2.3. Thermal constraints

In these calorimeters, the sample heater, sample, and thermometer are weakly thermally linked through two sets of electrical leads to a temperature controlled platform (inside the vacuum space) as shown in figure 3; the phosphor bronze electrical leads and stainless steel support post passing through the base of the calorimeter serve as the thermal link between the platform and the cryogenic bath. The platform heater power P_{PH} required to raise the platform temperature T_s a specific amount above the bath temperature T_b depends on the mean thermal conductance $\bar{K}$ of the platform to bath thermal link over that temperature range:

$$P_{PH} = \int_{T_b}^{T_p} K\,(T)\,dT = \bar{K}\Delta T \tag{1}$$

where $K(T)$ depends on the choice of materials and T_b depends on the fridge's cooling power.

From a practical standpoint, there are 3 key constraints on P_{PH} and hence $K(T)$: (1) stable PID temperature regulation for $T_p \geq 0.1$ K, (2) quick recovery of the dilution refrigerator for $T_p \leq 4$ K and (3) the ability to reach $T_p = 10$ K when neeed. In our operating environment, this requires $P_{PH} \gtrsim 20$nW at $T_p = 0.1$ K, $P_{PH} \leq 400\mu$W at $T_p = 4$ K, and $P_{PH} \leq 4$mW at $T_p = 10$ K. As shown in figure 4, the measured dependences of T_p on P_{PH} satisfy these 3 key constraints for both calorimeters. Moreover, by scaling the cross-sectional area of the leads passing through the calorimeter base to match the reduction in calorimeter length, we are also able to closely match the qualitiative and quantitative dependence of T_p on P_{PH} for the two calorimeters. We find that in both cases, T_p is well-described by the following power law function

$$T = T_0 + A(P_0 + P)^n \tag{2}$$

with $n \lesssim 0.5$. A and n depend only on the calorimeter; P_0 and T_0 also depend on the fridge.

3. Temperature Calibration in Magnetic Field

Prior to cross-calibration, the sample and platform thermometers were repeatedly thermally cycled between room temperature and 4.2 K (after mounting inside the calorimeter). Thermal cycling was deemed complete once both the room temperature and low temperature equilibrium values remained unchanged for 10 consecutive cycles (for a total of 60 cycles). The thermometers were cross-calibrated in zero field against a LakeShore CX1010SD Cernox between 0.1 K and 10

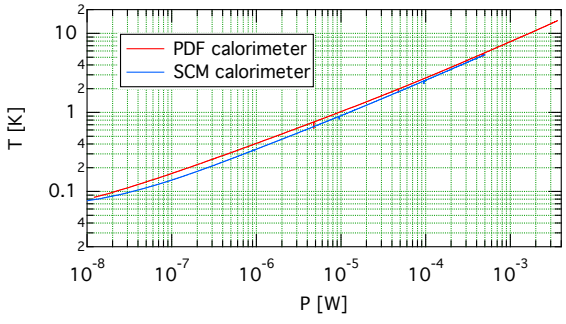

Figure 4. Platform temperature T_p as a function of platform heater power P_{PH} for the 45 tesla PDF and 18 tesla SCM field-rotatable small sample calorimeters. The calorimeters are designed for measurements between 0.1 K and 10 K. A heater power of 400 μW brings the interior to 4.2 K while the mixing chamber remains below 100 mK, allowing for easier and faster temperature regulation of the platform.

K and an Entropy Cryogenics Type D RuOx between 0.050 K and 7.5 K. This data was used to fit the temperature dependence of each resistive sensor to the Chebyshev function

$$\log R(T,B) = \sum_{n=0}^{N} c_n(B) t_n(x) \tag{3}$$

for $B = 0$, where x is a function of $\log T$ [20]. A set of platform heater power sweeps in fixed magnetic fields (starting from the same refrigerator base temperature) then allowed us to determine the fit coefficients A, n, T_0, and P_0 in Eq. 2 and the magnetic field dependence of $c_n(B)$ in Eq. 3. Thermomolecular-corrected measurements of ^{3}He vapor pressure [21, 22, 23] and sensor resistance were used to test the calibrations in liquid ^{3}He between 0.4 K and 1.4 K in magnetic fields up to 36 T.

4. Experimental Results

Angle-dependent calorimetric measurements by our group were the first to demonstrate the existence of a field-induced phase transition into a magnetically modulated phase within the superconducting state of the layered-structure heavy fermion $CeCoIn_5$ [2, 9].

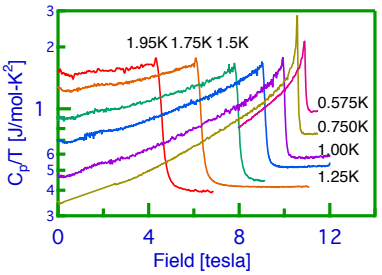

Figure 5. Field dependence of the specific heat of $CeCoIn_5$ above 0.5 K for H parallel to the highly conducting plane.

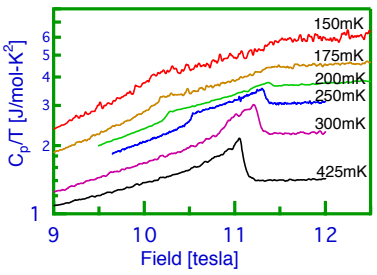

Figure 6. Lower temperature data revealing a field-induced transition to a new superconducting state below 0.35 K.

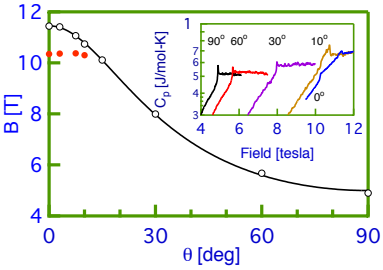

Figure 7. Magnetic-field orientation dependence of the high field phase for rotation out of the conducting plane.

As shown in Figs. 5, 6, and 7, the transition to the field-induced superconducting phase occurs for a narrow range of magnetic field at temperatures below 0.35 K when the field is directed along the [110] axis (parallel to the layers), but is quickly extinguished as the magnetic field is rotated out of the plane towards [001]. This may represent 'FFLO' enhancement of superconductivity due to the formation of electron spin domains; another interpretation attributes this field-angle-dependent phase transition to the onset of spin-density wave ordering [12].

More recently, we have investigated the field-angle dependence of magnetic-field-induced phases in a number of frustrated triangular-lattice $S = \frac{1}{2}$ quantum Heisenberg antiferromagnets with weak xy anisotropy, including $Ba_3CoSb_2O_9$, Cs_2CuCl_4 and Cs_2CuBr_4 [24]. Three magnetic phases are expected [25], each corresponding to a different spin arrangement: a low field 'Y' phase, an intermediate 'up - up - down' phase, and a high field 'V' phase. In angle-dependent measurements up to 36 T on $Ba_3CoSb_2O_9$, we have discovered (1) that the 'Y' and 'V' phases split into alternating and non-alternating co-planar subphases, (2) that contrary to previous reports, multiple field-induced phases occur for H $\parallel$ c as well, and (3) that the field-induced phases seen for these two orientations are in fact related to each other. The angle-dependence of these field-induced antiferromagnetic phases at 0.350 K is shown in Fig. 8. Details will be published elsewhere.

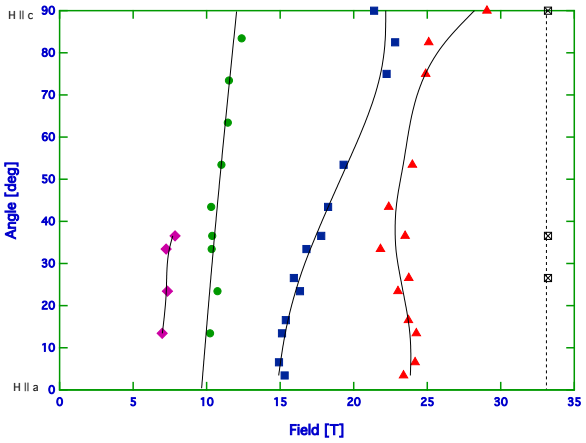

Figure 8. The angle-dependence of field-induced antiferromagnetic phases for field rotation from H||a ($\theta = 0°$) to H||c ($\theta = 90°$) for $Ba_3CoSb_2O_9$, an S = $\frac{1}{2}$ triangular-lattice Heisenberg antiferromagnet. The lowest and highest phases of the expected three phases — a 'Y' phase, an 'uud' phase, and a 'V' phase — split into alternating and non-alternating coplanar subphases in this system. The solid lines are guides to the eye indicating the evolution of each phase with field-angle; the dashed line represents the saturation field of 32.5 tesla.

Acknowledgments

A portion of this work was performed at the National High Magnetic Field Laboratory, which is supported by National Science Foundation Cooperative Agreement No. DMR-1157490, the State of Florida, and the U.S. Department of Energy. NAF was supported by NHMFL Visiting Scientist Grant 12411.

References

[1] Bondarenko V A, Tanatar M A and Kovalev A E 2000 *Review Of Scientific Instruments* **71** 3148
[2] Hannahs S T and Fortune N A 2003 *Physica B-Condensed Matter* **329-333** 1586–1587
[3] Deguchi K, Ishiguro T and Maeno Y 2004 *Review Of Scientific Instruments* **75** 1188
[4] Alicea J, Chubukov A V and Starykh O A 2009 *Physical Review Letters*
[5] Agosta C C, Jin J, Coniglio W A, Smith B E and Cho K 2012 *Physical Review B*
[6] Vorontsov A and Vekhter I 2007 *Physical Review B* **75** 224501
[7] Boyd G, Hirschfeld P, Vekhter I and Vorontsov A 2009 *Physical Review B* **79** 064525
[8] Das T, Vorontsov A B, Vekhter I and Graf M J 2013 *Physical Review B* **87** 174514
[9] Radovan H A, Fortune N A, Murphy T P, Hannahs S T, Palm E C, Tozer S W and Hall D 2003 *Nature* **425** 51–55
[10] Deguchi K, Mao Z, Yaguchi H and Maeno Y 2004 *Physical Review Letters* **92** 047002
[11] An K, Sakakibara T, Settai R, Onuki Y, Hiragi M, Ichioka M and Machida K 2010 *Physical Review Letters* **104** 037002
[12] Tokiwa Y, Bauer E D and Gegenwart P 2012 *Physical Review Letters* **109** 116402
[13] Kovalev A E, Ishiguro T, Yamada J, Takasaki S and Anzai H 2001 *Journal of Experimental and Theoretical Physics* **92** 1035–1037
[14] Malone L, Taylor O J, Schlueter J A and Carrington A 2010 *Physical Review B* **82** 014522
[15] Beyer R and Wosnitza J 2013 *Low Temperature Physics* **39** 225–231
[16] Palm E C and Murphy T P 1999 *Review Of Scientific Instruments* **70** 237–239
[17] Fortune N A, Eblen M A, Uji S, Aoki H, Yamada J, Tanaka S, Maki S, Nakatsuji S and Anzai H 1999 *Synthetic Metals* **103** 2078–2079
[18] Sullivan P and Seidel G 1968 *Physical Review* **173** 679–685
[19] Bachmann R, DiSalvo F J, Geballe T H, Greene R L, Howard R E, King C N, Kirsch H C, Lee K N, Schwall R E, Thomas H U and Zubeck R B 1972 *Review Of Scientific Instruments* **43** 205–214
[20] Fortune N A, Gossett G, Peabody L, Lehe K, Uji S and Aoki H 2000 *Review Of Scientific Instruments* **71** 3825–3830
[21] Rusby R L 1985 *Journal of Low Temperature Physics* **58** 203–205
[22] Rusby R L and Durieux M 1984 *Cryogenics* **24** 363–366
[23] Roberts T R and Sydoriak S G 1956 *Physical Review* **102** 304–308
[24] Fortune N, Hannahs S T, Yoshida Y, Sherline T, Ono T, Tanaka H and Takano Y 2009 *Physical Review Letters* **102** 257201–257204
[25] Chubukov A V and Golosov D I 1991 *Journal Of Physics-Condensed Matter* **3** 69–82